D-V2X: Exploring DECT NR+ for 5G NR Vehicular Ad-Hoc Networks Beyond C-V2X

Jannusch Bigge and Christoph Sommer
TU Dresden, Faculty of Computer Science, Germany
https://www.cms-labs.org/people/ { bigge , sommer }

***Abstract*—We refer to a technology stack employing DECT NR+ for vehicular communication as *D-V2X*, emphasizing that DECT NR+ is compatible with (and exploits features of) 5G NR of Cellular Vehicle-to-Everything (C-V2X), but – unlike C-V2X – it was designed to operate in unlicensed spectrum and without infrastructure support in a true ad-hoc manner. Yet, despite its promising characteristics, DECT NR+ remains unexplored for vehicular communication. Our system-level simulation study demonstrates that DECT NR+ can be a viable basis for vehicular communication, achieving communication windows of approximately 10 s for relative speeds of 120 km/h. Our work also reveals many open research questions that require investigation. We also describe the design and validation of the underlying first publicly available open-source physical/MAC layer model of DECT NR+. We based it on the well-established Veins framework for vehicular network simulation, enabling researchers to evaluate DECT NR+ performance in realistic traffic scenarios. We validate the model through both analytical comparison with the standard and experimentally using real hardware.**

I. Introduction

While 5G can offer high-bandwidth or ultra-reliable links for diverse use cases, it can perform poorly for point-to-point vehicular communication in Cellular Vehicle-to-Everything (C-V2X) scenarios: Sidelink communication in Mode 1 requires base station coordination for resource allocation, and coverage focuses on ground-level networks. Sidelink communication in Mode 2 enables direct device-to-device communication without base station coordination through autonomous resource selection. Yet, it experiences performance degradation at vehicular speeds, particularly due to shorter contact durations and increased interference at higher speeds [1]. Furthermore, in either case C-V2X was designed to operate in licensed spectrum, creating a dependency on service providers and increasing license costs.

The ETSI ITS-G5 and IEEE WAVE standards – both based on IEEE 802.11p – are often considered as the alternative solution, but they require different hardware than 5G, complicating seamless integration with C-V2X.

Yet, this might be a false dichotomy. The European Telecommunications Standards Institute (ETSI) defined DECT-2020 NR [2] (marketed as DECT NR+) as a non-cellular 5G system based on the DECT[1] standard family and the 5G New Radio (NR) physical layer.

DECT NR+ achieves functional compliance with 5G while enabling operation without dedicated base stations and reusing existing 4G/5G hardware (with modified firmware as shown by the nRF9151 DK), providing a low-cost entry point into the 5G technology stack. Crucially, every device can act as a local base station, dynamically assigning resources to other devices, while simultaneously functioning as a client. This can enable license-free ad-hoc networks with fast channel access even under high node density and thus complement existing 5G networks.

These characteristics make DECT NR+ appear particularly well-suited for vehicular ad-hoc networks: infrastructure-free operation can enable communication in areas without cellular coverage, deterministic channel access can eliminate contention-based delays, and dynamic resource allocation can support high vehicle densities while maintaining low latency – key requirements for safety-critical V2X applications. At the same time, the technology stack remains compatible to 5G and uses a license-free band to enhance independence and resilience.

We refer to such a technology stack employing DECT NR+ in vehicular scenarios as *D-V2X*.

Despite its promising characteristics, DECT NR+ remains unexplored for vehicular communication. Existing research relies mainly on analytical approaches or MATLAB-based link-level models only, and limits system-level performance evaluation in realistic scenarios to such with a focus on smart home applications. While a DECT NR+ simulator exists, it is not publicly available, creating a substantial barrier for researchers and practitioners seeking to explore its potential for V2X applications.

This paper makes two fundamental contributions:

1) We describe the design and validation of the (to the best of our knowledge) first publicly available open-source[2] DECT NR+ physical/MAC layer model designed for system-level vehicular network simulation.
   We based it on (and integrate it with) the well-established Veins framework for vehicular network simulation. This allows research to move beyond isolated simulations of individual features and can provide a foundation for reproducible DECT NR+ research all the way up to system-level studies.
   Validation encompassed both *(1)* analytical comparison against the standard as well as *(2)* real-world measure-

[1]The acronym *DECT* has undergone various (re-)interpretations over time, both in its standards and in commercial use, finally settling on *Digital Enhanced Cordless Telecommunications*.

[2]https://www.cms-labs.org/research/software/dv2x

17th IEEE Vehicular Networking Conference (VNC 2026)

ments using nRF9151 DK development kits from Nordic Semiconductor and an Ettus USRP B210 (B210) Software Defined Radio (SDR).
2) We demonstrate the potential of DECT NR+ for V2X applications in a system-level simulation study. Our results show robust communication windows at relative speeds up to 260 km/h with varying numerologies, but also highlight many future research avenues.

II. Fundamentals of DECT NR+

ETSI created DECT NR+ as a non-cellular wireless system with a focus on Ultra-Reliable Low-Latency Communication (URLLC) and Massive Machine-Type Communication (mMTC) [2]. DECT NR+ operates in unlicensed spectrum bands, primarily in the 1880–1920 MHz range (varying by region), eliminating spectrum licensing costs and enabling deployment without regulatory approval.

The basic structure consists of 10 ms frames divided into 24 slots (maintained for backward compatibility with legacy DECT, DECT evolution, and DECT ULE systems that share the same spectrum). This results in a slot duration T_{slot} of 0.416 67 ms. The reference time for frame alignment is provided by a *notional clock* [2, Part 2, 5.5.1]. Slots are further divided into subslots, where each subslot consists of 5 Cyclic Prefix Orthogonal Frequency Division Multiplexing (CP-OFDM) symbols. The length of a CP-OFDM symbol is determined by the subcarrier scaling factor (μ), which results in a different number of subslots per slot: Values of $\mu = 1$, $\mu = 2$, $\mu = 4$, or $\mu = 8$ configure 2, 4, 8, or 16 subslots per slot, respectively. Figure 1 shows a frame for $\mu = 1$ (resulting in 48 subslots).

A Time Division Multiple Access (TDMA) approach combined with Time Division Duplex (TDD) addresses limitations of Carrier Sense Multiple Access (CSMA) based protocols by addressing the collision problem proactively instead of reactively to allow deterministic channel access times.

The spectrum is divided into channels of 1.728, 3.456, or 6.912 MHz in a Frequency Division Multiple Access (FDMA) manner. The transmission bandwidth is determined by both μ and the Fourier transform scaling factor (β), where β can be 1, 2, 4, 8, or 16. Together, they scale the base bandwidth of 1.728 MHz, resulting in bandwidths from 1.728 MHz (with $\mu = 1$ and $\beta = 1$) to 221.184 MHz (with $\mu = 8$ and $\beta = 16$). To support these kinds of wide bands, multiple channels are combined. The channel raster depends on the used band and is either 0.864, 1.728, or 2 MHz.

To enhance reliability, DECT NR+ supports Hybrid ARQ with incremental redundancy and 11 Modulation and Coding Schemes (MCSs). This adaptability enables the standard to provide robust connections when reliability is critical – or high-throughput connections when channel conditions permit. Additionally, DECT NR+ supports up to 4×4 Multiple-Input Multiple-Output (MIMO) configurations. All those features result in transmission speeds starting at a throughput of 0.326 Mbit/s and increasing up to multiple Gbit/s.

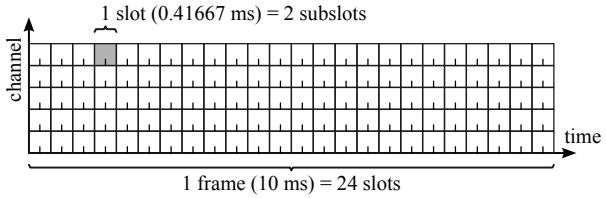

Figure 1. DECT NR+ frame structure with the subcarrier scaling factor (μ) set to 1 (resulting in two subslots per slot).

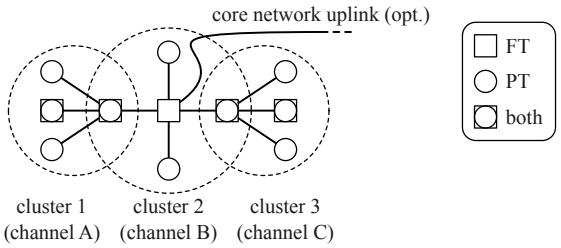

Figure 2. Multi-cell network with one device accessing a 5G network via the Trusted Non-3GPP Gateway Function (TNGF).

DECT NR+ supports multiple networking architectures through two *operational modes*. Each device can enable Fixed Terminal (FT) mode, Portable Terminal (PT) mode, or both simultaneously. In FT mode, a device functions as a base station, coordinating radio resources for its cell. In PT mode, a device receives resource assignments from the FT device it is in association with. A single device can participate in multiple cells simultaneously.

These operational modes enable diverse network topologies: wireless point-to-point and point-to-multipoint links provide direct device-to-device communication, while single-cell and multi-cell topologies support networks with one or more devices in FT mode. Mesh networks are also supported, as illustrated in Figure 2.

DECT NR+ also includes interworking profiles for integration with 3GPP 5G networks, either as an untrusted non-3GPP access network to the Core Network via the Non-3GPP Inter-Working Function (N3IWF), or as trusted access network via the Trusted Non-3GPP Gateway Function (TNGF). Depending on the configuration, a DECT NR+ device can function as an intelligent gateway or as User Equipment (UE), promising to allow existing 5G systems to be enhanced with fast, ultra-reliable ad-hoc networks at low cost.

III. Related Work

Existing DECT NR+ research relies predominantly on MATLAB-based physical and link-level simulation models and limited real-world testing. Penner et al. [3] investigated link-level performance using a standard ITU-R [4] channel model in MATLAB, demonstrating that DECT NR+ fulfills URLLC criteria (99.999 % reliable user plane latency of less than 1 ms and one million devices per square km).

Their work also provides results to calibrate physical layer performance curves. Building on this foundation, Llaguno et al. [5] investigated two factory automation use cases, concluding that the physical layer alone is insufficient for URLLC – and speculate that MAC layer mechanisms are also required to fulfill those demands.

Samuylov et al. [6] investigated MAC layer mechanisms for mMTC with respect to Packet Delivery Ratio (PDR), concluding that MAC layer mechanisms are necessary for reliable mMTC as well. Kovalchukov et al. [7] investigated DECT NR+ stability regarding packet loss as a function of device density, demonstrating robust performance due to the combination of a modern physical layer and advanced MAC layer mechanisms. They used the WINTERsim simulator for their evaluation. Nihtilä and Berg [8] focused on energy consumption in mesh networks with battery-powered Internet of Things (IoT) devices in mind, creating a model for ns-3 that, to the best of our knowledge, is not publicly available.

Real-world testing of DECT NR+ remains limited. Graf et al. [9] conducted multiple real-world tests across diverse environments (indoor: industrial and office; outdoor: urban and rural) using the nRF9161 (the predecessor of the hardware used in our experiments), focusing on device power consumption. Mudriievskyi et al. [10] investigated round-trip time as a latency measurement, focusing on COTS hardware (again the nRF9161). Waßmann et al. [11] performed a field test in an industrial environment using two B210s, focusing on error rate under different numerologies, channels, and bandwidths.

Beyond performance evaluation, DECT NR+ has also been explored as a building block for new applications. Dang et al. [12] created EWDC, an Apple Wireless Direct Link (AWDL)-like technology where the Bluetooth Low Energy (BLE) component is replaced by DECT NR+, using the nRF9161 DK to build a testbed.

Summing up, to the best of our knowledge, research so far has been limited to link-level studies or small-scale real-world tests, and has limited reproducibility. In addition, no work has explored vehicular scenarios. We fill this gap by describing a doubly (in real-world experiments and analytically, against reference values) validated simulation model for the physical layer and parts of the MAC layer for the widely used simulation framework Veins [13]. We employ it to conduct first experiments on how a D-V2X stack employing DECT NR+ may perform in a vehicular context. We make the model publicly available as open-source software to encourage future research while simultaneously constantly developing it further.

IV. Simulation Model

To investigate DECT NR+ performance – the foundation for our system level D-V2X simulation – we created a simulation model for Veins [13], a well-established network simulator focused on vehicular communication. Compared to other frameworks, this allows us to strike a balance in the level of abstraction between performance and granularity. Our implementation runs on OMNeT++ 6.3.0 and, as shown in Figure 3, follows the modular design of Veins where the

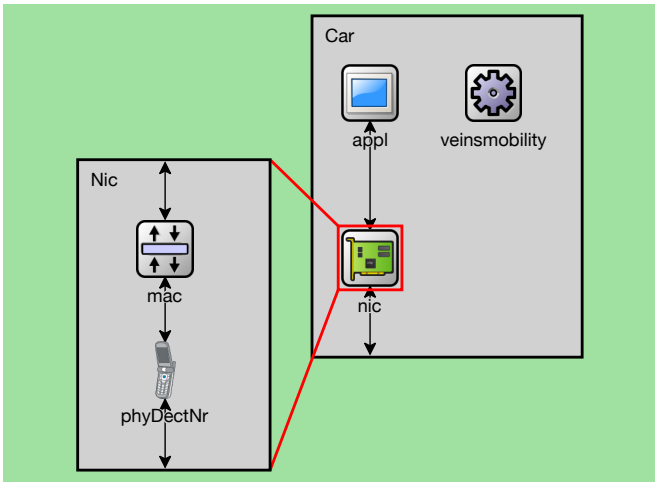

Figure 3. View of the simulation modules. The DECT NR+ Network Interface Card (NIC) consists of two submodules – the physical layer and the MAC layer. The application can be any Veins module that implements the Application Interfaces.

DECT NR+ Network Interface Card (NIC) consists of two submodules (representing the physical layer and the MAC layer) and is modeled independently from the *application* module (which represents the rest of the stack and we hence term to send *packets*).

We focus on the physical layer, implementing it at the level of individual CP-OFDM symbols but without modeling the mapping of individual Bits, which is sufficient for our current simulation that focuses on whether a packet is broken and not which part is broken. The underlying channel model allows us to select which frequencies of the spectrum to simulate. From the overall spectrum of the symbol, we focus on the center and the outer frequencies, as our current model assumes that the signal of every symbol is evenly distributed over the allocated spectrum with the same power and aligns with the channel raster. Thus, for calculating whether we can receive a symbol successfully, it is sufficient to focus on the center frequencies of potential colliding symbols as they either perfectly align or do not interfere at all, thus substantially speeding up the simulation [14]. With minor modifications, it would be possible to simulate each subcarrier individually, which would substantially increase computational load but enable more detailed investigations of dense channel raster effects with wider bands.

We focused on single-input single-output systems, although DECT NR+ supports up to 4×4 MIMO. Similarly, Hybrid ARQ, an optional yet highly beneficial feature, is not currently implemented.

Our implementation follows the DECT NR+ standard specifications for all implemented features, supporting all bands, channels, numerologies, and MCSs defined by the standard.

MAC layer functionality is limited to channel scanning, resource selection, and standard compliant access via TDMA and TDD. Currently missing is the creation and handling of *associate* messages, both in FT and PT mode; thus, in the

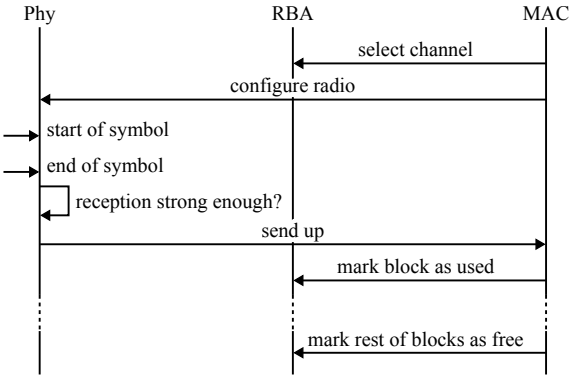

Figure 4. Overview of the background scanning process running continuously in the MAC layer. The process follows the procedure described in the standard [2, Part 4, Section 5.1.2].

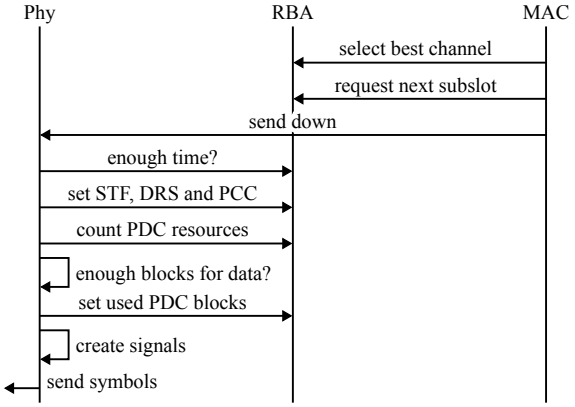

Figure 5. Overview of the sending process. The MAC layer is responsible for the alignment with subslots in the time domain and for the selection of the best possible channel. This is based on the information stored in the Resource Block Allocator (RBA). The physical layer first allocates the individual blocks to determine how many blocks in the Physical Data Channel (PDC) are available for actual data. If the data fits, the physical layer creates the final signals of each symbol for transmission.

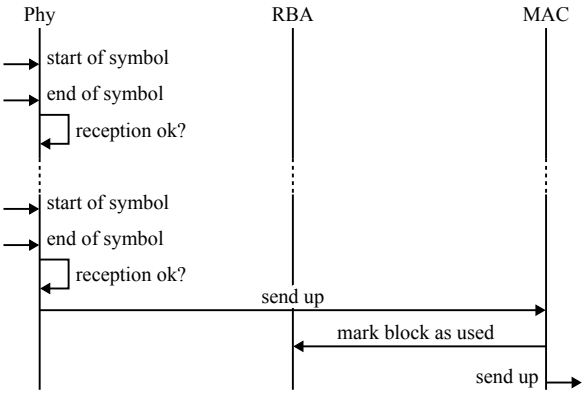

Figure 6. Overview of the receiving process. For each arriving symbol, the physical layer consults its *decider* component whether it can be received. If all symbols were received successfully, the packet is forwarded to the MAC layer.

current implementation each device must decide for itself which resources to use.

The radio resource allocation (including the TDD mapping and the channel load of the individual subslots per channel) is stored and managed by the MAC layer in the Resource Block Allocator (RBA). It also provides basic functionality to query the next free subslot or to check how many subslots are left in the TDD.

The channel and subslot selection procedure – as described in Figure 4 – is initiated by each node as soon as their mode is set to FT. The physical layer reports every incoming symbol to the MAC layer, which then marks the active subslot in the channel with the corresponding state (*busy* or *possible* as defined in the standard) in the Resource Block Allocator (RBA). After the minimum scan time, every block that was not marked otherwise gets updated to *free*.

Figure 5 illustrates the process of sending. After selecting the best channel based on the information provided by the RBA, the MAC checks for the next available subslot and sends – aligned to the start of it – the packet to the physical layer. The MAC layer configures the active channel with the corresponding numerology information for the physical layer. The physical layer only has access to this one active channel from the RBA to allocate the individual blocks and to perform additional checks if the packet passed by the MAC layer fits into the available subslots. This shared approach allows the MAC layer to manage the complete access scheme in the time and frequency domain, while the physical layer can update the resources on actual events without potential synchronization issues.

Figure 6 illustrates the procedure of receiving a transmission. The received signal strength of each symbol is computed using the channel and antenna models provided by Veins. Reception is modeled using binary erasure: a decider module within the physical layer compares the received signal strength against a fixed threshold value. Symbols above the threshold are received successfully, while those below are discarded. If we received all symbols of a packet successfully, the packet is forwarded to the MAC layer. This is a simplification that is valid for the simulation study in this paper, where interference plays no role: We only simulate two cars that either send in the same slot (thus trying to receive while sending, which is not possible) or send in different slots (thus without anyone else sending during this time).

Our complete implementation (which also underlies the system level performance evaluation presented in this paper) is openly available[2, page 1] to enable reuse and facilitate ongoing research. Work is ongoing to support additional features and future research lines identified by our study.

V. Validation

We validated our simulation model both analytically and experimentally. For the analytical validation, we compared simulation results against reference values for different physical layer configurations provided in the standard. Additionally, we

conducted an experimental real-world study to verify these results to the extent that the available hardware permitted.

A. Validation Against the Standard

For the validation of our simulation against the standard we ran two simulations: We used the first simulation to perform unit tests and smoke tests under a wide range of conditions and the second simulation to run throughput tests for comparison with the reference values from the standard.

We tested that the physical layer applies changes according to the provided numerology and that block allocation conforms to the standard with respect to those changes – depending on the length of the data and the used MCS, the actual needed number of blocks in the Physical Data Channel (PDC) differs. We also checked that the calculated timings are correct.

In Figure 7, we show a fraction of the debug output (created by the test for the resource block allocation) in the same way as provided by the standard [2, Part 3, Figs. 4.5-2 and 4.5-3]. The standard provides allocations for 1, 2, and 4 subslots with $\mu = 1$ and $\beta = 1$, including configurations with up to eight effective antennas (spatial streams), allowing direct comparisons of the obtained values. The configuration of the physical layer defines the number and position of the Demodulation Reference Signals (DRSs) as well as the length of the Synchronization Training Field (STF) and Guard Interval (GI). Based on this pre-filled raster, a fixed number of Physical Control Channel (PCC) blocks are evenly distributed in the first OFDM symbols and the PDC blocks are placed in the remaining free blocks. We validated other values of β, μ, and number of spatial streams through manual calculations.

In addition to the physical layer, we also performed multiple unit tests on the RBA: returning the correct number of free subslots, performing correct allocation, returning the correct start time, and applying changes with changing numerologies.

In addition to unit tests, we also used smoke tests to verify that sending, the timings, collisions on the wireless channel, and the general procedure (from creating data in the application layer to receiving it in the application layer) are performing as expected.

We conducted a second simulation study to obtain values for the throughput that we compared against the reference values from the standard's appendix [2, Part 3, Annex C]. The standard provides values for the Transport Block (TB) size and for the maximum data rate, but, again, only for a limited number of configurations: now for all combinations of μ, β, and MCS but only for transmissions with a length of 1, 2, or 4 slots with one spatial stream. We extended those reference values to all possible slot lengths, as those change the overhead per frame. All values were measured under ideal conditions in our simulation.

With the throughput test we measured the size of the TB resulting from the number of available PDC blocks to verify that our algorithms allocate the correct number of PDC blocks for every configuration. Based on the TB size, we then calculated the data rates depending on the MCS to compare them against the reference values from the standard.

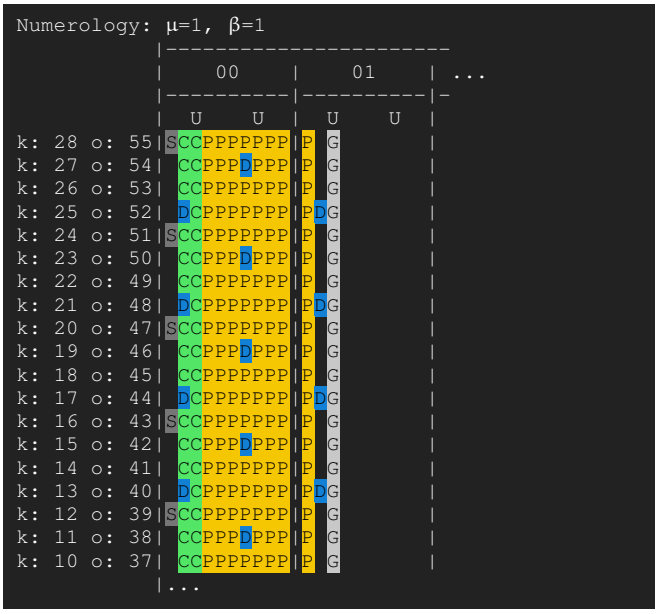

Figure 7. Excerpt from a block allocation map as rendered by the debug output of a simulation for comparison with the standard. Shown is an allocation for $\mu = 1$ and $\beta = 1$, for a two-slot transmission with one spatial stream and 100 bit payload with MCS = 0. Numbers and letters in the column headers indicate the slot number and Time Division Duplex (TDD) allocation, respectively. Colored upper-case letters indicate the different kinds of resource allocation.

Figure 8. Experimental setup of two nRF9151 DK and an Ettus USRP B210 Software Defined Radio (SDR) doing a throughput test. The SDR is capturing the signal and plotting a spectogram with GNU Radio.

Before we turn to the evaluation of the validation, we first describe the real-world experiment.

B. Validation Against Real-World Experiments

For our real-world experimental validation, we used two Nordic nRF9151 DK boards (the successor of the nRF9161 DK used in most other real-world DECT NR+ studies), along with a B210. The experimental setup for the real-world experiments is shown in Figure 8.

We used firmware version v1.1.0, which we directly requested from Nordic Semiconductor, as required. The firmware is identical for the nRF9151 and the nRF9161.

The firmware supports bands 1, 2, 4, 9, and 22 with MCSs 0 through 4 for $\mu = 1$ and $\beta = 1$, a bandwidth of 1.728 MHz, and a single spatial stream, resulting in a maximum achievable throughput of 2.6 Mbit/s – a small fraction of the possible multiple-Gbit/s data rates, but sufficient for validation.

Nordic provides several example applications for their devices that can be flexibly parameterized. One of these is a throughput performance test (accessible via the *perf* command in the *DECT shell* – an example application provided by Nordic to test various physical layer features), which operates in a client–server configuration. The client initiates the test and then continuously transmits packets to the server, which reports statistics about the received data upon completion.

We configured the application to match the example scenario described in the standard [2, Part 3, Annex C]. Due to software limitations of the devices, we could only test a subset of packet lengths: Without modifying the application, only header length type 0 is used, which specifies packet length in subslots, but the application only allows setting the length in slots. Thus, with a configured length of 8 and $\mu = 1$ (two subslots per slot), the total packet length is 16 subslots – the maximum allowed length by the standard.

We used the B210 to observe the timing behavior and the spectrum allocation of the nRF9151 DK to validate the actual channel usage in both time and frequency domain (and not only the absolute values in packet throughput) against our simulation model. We used a *USRP* source block in *GNU Radio Companion* to record the data.

With measurement values collected by a) simulation studies and b) real-world experiments, we compare them in the next subsection to validate that our model conforms to the standard.

C. Evaluation

As shown in Figure 9, the results from all three – the standard, the experiment, and the simulation – match perfectly for all obtainable values (the standard provides reference values for packet lengths of 1, 2, and 4 slots [2, Part 3, Annex C]). The data rate increases logarithmically with packet length until the first packet length that is not a divisor of 24. At this point the frame cannot be fully filled, leading not only to differences in throughput due to overhead but also due to unused subslots. The general logarithmic behavior results from reduced overhead when transmitting longer packets, as the STF and PCC do not change in size, leading to more available blocks for the PDC. With a packet length of 12 slots, we achieve the highest data rate.

If we combine packets of different lengths and fill the complete frame (24 slots), the combination with the lowest overhead would be the maximum packet lengths of 16 and 8 slots. With this combination, we could send 6016 kbit per frame, which is only slightly higher than the highest measured 6000 kbit per frame with two 12-slot long packets, as shown in the figure.

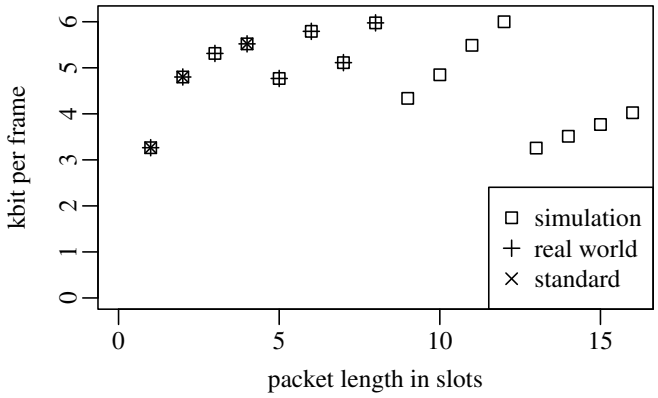

Figure 9. Cross-validation of the allocated data symbols in kbits (per frame!) depending on packet length for three different approaches: reference values provided by the standard, simulation results from our model, and experimental results obtained with nRF9151 DK hardware. With a fixed packet length, the data rate (per frame) was investigated with the subcarrier scaling factor (μ) set to 1, the Fourier transform scaling factor (β) set to 1, and the Modulation and Coding Scheme (MCS) set to 0. All three approaches show matching results for the possible configurations.

In Figure 10 we show the spectrum allocation of a single slot transmission with a completely filled TB followed by a single gap slot. As $\mu = 1$ defines a slot length T^{μ}_{subslot} of 416.67 µs and a symbol time T^{μ}_{symbol} of 41.667 µs with a GI of $\frac{4}{9} \times T^{\mu}_{\text{symbol}} = 18.52\,\mu\text{s}$, the actual occupied time of the subslot is only 398.15 µs, matching our measurements. With these results, we validated that the durations and the actual used bandwidth align with our model.

VI. D-V2X Simulation Study

Based on the validated model, we created a simulation study to investigate potential system-level performance. Our main focus is the achievable communication time between vehicles under varying speeds.

As illustrated in Figure 11, we simulate two cars driving on a straight road in opposite directions at constant speed. Each car transmits beacon packets that are created in the application layer in fixed intervals of 1 ms, at time $T_{\text{send},i} = T_{\text{start}} + i \times 1\,\text{ms}$ with $i \in \mathbb{N}$. The initial start time T_{start} is drawn by the application layer from a uniform distribution between 0 and the duration of a frame $T_{\text{frame}} = 10\,\text{ms}$.

As we cannot transmit across the frame boundaries, we need to make sure that every transmission finishes within the frame. Therefore, we cannot start a transmission in the last subslot, and for $\beta = 1$ (that is, packets are two subslots long) also not in the second-to-last subslot. Thus, we need to choose T_{start} such that never $T_{\text{frame}} > T_{\text{send},i} \geq T_{\text{frame}} - j \times T^{\mu}_{\text{subslot}}$ with $j = 2$ if $\beta = 1$ else $j = 1$ for any $i \in \mathbb{N}$.

The beacon packet contains no user data from the application layer and is constructed as a DECT NR+ broadcast packet without encryption using Dedicated Traffic Channel (DTCH) number 1, leading to a final MAC packet size of 8 Byte. Both nodes enable FT and PT mode at the same time, thus are responsible for radio resource selection.

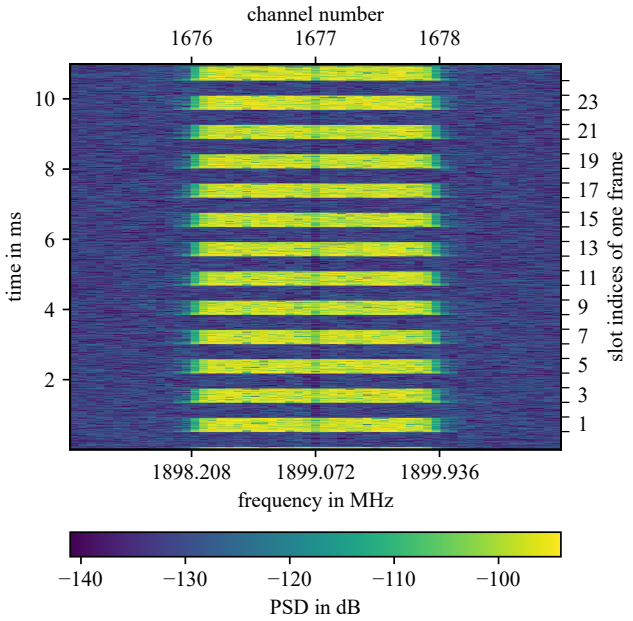

Figure 10. Spectrogram of one frame alternating between a packet and a gap for each slot on channel 1677 with a transmission bandwidth of 1.728 MHz in a channel raster of 0.864 MHz. The data was sent by an nRF9151 DK and recorded by an Ettus USRP B210 tuned to 1899.072 MHz

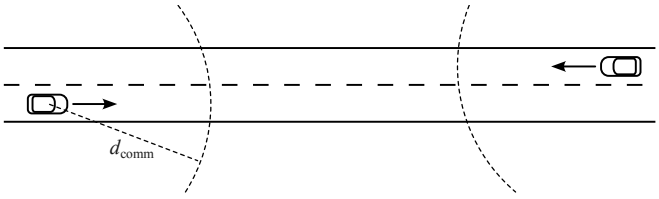

Figure 11. Simulation setup: Two cars are driving in opposite lanes on a road. Their active communication time (how long they can communicate with each other) depends on their speed and the effective communication range d_{comm}, which is dictated by effective transmission power, path loss, and receiver performance.

The MAC layer automatically aligns transmissions from the application layer to uplink subslots. Transmission power is set to 100 mW to match the hardware, although 200 mW would also be within specification and would increase communication range and thus active communication time.

We tested all values of μ, as higher values result in shorter symbol durations for the same data length, thereby occupying less frame time and potentially reducing the chance that both transmissions fall into the same subslot.

Each configuration was repeated 100 times with relative speeds between the two cars of 60, 120, and 260 km/h.

Upon successful reception of a beacon packet, the receiver records the time of reception and the current location in the application layer. In the same manner, the sender records the sending time and the sending location after creating the packet.

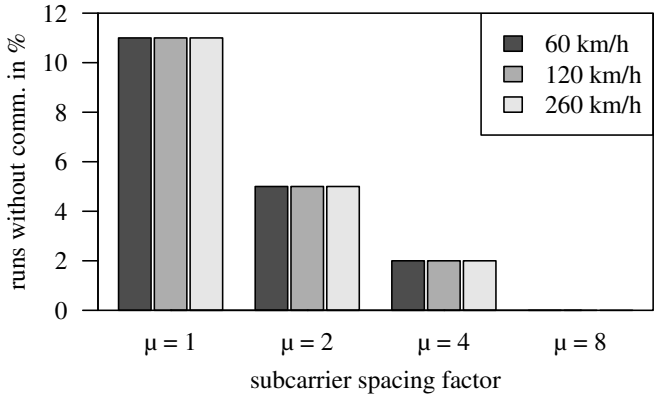

Figure 12. Bar chart showing the percentage of failed simulation runs in relation to the subcarrier scaling factor (μ) and the relative speed of the cars. Increasing μ reduces collisions, down to approx. zero for $\mu = 8$. Speed has no influence on the values.

VII. Results for the D-V2X Study

For the evaluation, we focused on two metrics: The first metric is the number of runs without any successful communication at all. The reason for the existence of such runs is straightforward: Both cars perform standard-compliant channel scanning and resource selection while still out of range of each other, so both independently select the same channel. The only difference is the initial (random) offset T_{start} chosen by the application layer, which leads to different selections of subslots by the MAC layer to align the sent-down packets with the TDMA scheme. If both applications choose a T_{start} that gets aligned into the same subslot we have a collision. As the current MAC layer implementation has no feedback mechanism to verify whether a transmission was successful or not, there is no way to trigger resource rescheduling. Thus, in our scenario, each run results in either zero collisions or persistent collisions throughout. We therefore report the fraction of runs without any successful communication.

Figure 12 shows the results. The fraction of unsuccessful runs is independent of the speed of the cars and decreases with increasing μ as we have more subslots to choose from (which makes it more unlikely that two packets get aligned into the same subslot within a frame by the MAC layer). As β is set to 1 (every packet needs to be two subslots long), $\mu = 1$ would theoretically result in a collision chance of $\approx 6.57\,\%$. As one can see in the figure, the measured number of runs that have no successful communication is much higher. The main reason is that we have the additional limitations discussed above for T_{start} and not only the last or second-to-last subslot – depending on β – is blocked for sending.

For $\mu = 8$ the theoretical chance of a collision with perfect alignment and a packet length of two subslots would be 0.78 %: As we have 384 subslots with 383 possible start positions selected by two nodes we have $383^2 = 146689$ possible combinations. Two transmissions – starting at i and j – overlap if $i = j$ (exact same slot) or $i = j - 1$ (node two starts one slot earlier) or $i = j + 1$ (node two starts

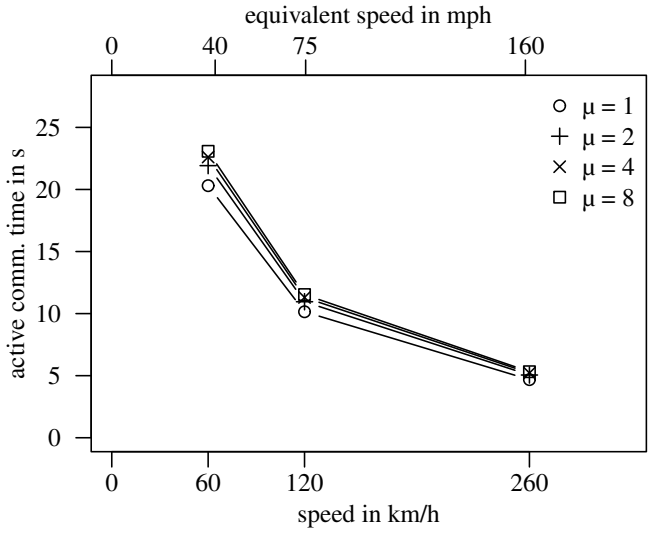

Figure 13. Active communication time of two cars meeting on the road; for different relative speeds and for different values of the subcarrier scaling factor (μ). Values are plotted for a reduced transmit power of 100 mW (instead of the maximum possible 200 mW defined by the standard for Class I devices).

one slot later). If we count the overlaps we get 1144 in total: with $i = 1$ we overlap if $j \in \{1, 2\}$ (two overlaps), with $2 \leq i \leq 382$ we overlap if $j \in \{i - 1, i, i + 1\}$ (three overlaps each), and with $i = 383$ we overlap if $j \in \{382, 383\}$ (two overlaps). Therefore, the probability of a collision is the number of possible overlaps divided by the total number of positions: $1144/146689 = 0.0078$. As we only simulate with 100 repetitions, it is plausible that for $\mu = 8$ we see zero unsuccessful runs in our simulation study.

The second metric is the active communication time, defined as the duration between the first and last successfully received packet. As we only have two communication partners in our scenario and only distance and scheduling impact packet loss, a reception gap in between the first and the last successful received packet would be very rare. In fact, none of our simulation runs experienced this, so calculation of the metric is straightforward.

In Figure 13, we can see that even under high speeds the active communication time is over ≈ 5 s, rising to $\approx$ 20–23 s at lower speeds. The spread of the average communication time between the smallest μ and the highest one shrinks with increasing speed. This spread is caused by the runs without successful communication. The active communication time then is zero; thus, the average is lower.

VIII. Conclusion and Future Work

In this paper, we investigated DECT NR+ as a promising technology for vehicular ad-hoc networks. We refer to a technology stack employing DECT NR+ for vehicular communication as *D-V2X*, emphasizing that DECT NR+ is compatible with (and exploits features of) 5G New Radio (NR) of Cellular Vehicle-to-Everything (C-V2X), yet – unlike C-V2X – it was designed to operate in unlicensed spectrum and without infrastructure support in a true ad-hoc manner.

Our system-level simulation study demonstrated that DECT NR+ can be a viable basis for vehicular communication, achieving communication windows of ≈ 10 s for relative speeds of 120 km/h. Our work also revealed many open research questions that require investigation.

We also described the design and validation of the underlying first publicly available open-source[2, page 1] physical/MAC layer model of DECT NR+. We based it on the well-established Veins framework for vehicular network simulation, enabling researchers to evaluate DECT NR+ performance in realistic traffic scenarios. We validated the model via analytical comparison with the standard and experiments with real hardware.

Future work will focus on advanced MAC layer functions, investigating channel allocation and selection (previously only proven in static scenarios) in dense traffic scenarios and those characterized by high topology dynamics – and work on the model continues in order to support such research.

References

[1] M. Tabassum and A. Oliveira, "5G NR sidelink time domain based resource allocation in C-V2X," *Elsevier Vehicular Communications*, vol. 53, p. 100 902, Jun. 2025.

[2] "DECT-2020 New Radio (NR); Release 2; Parts 1 to 5," ETSI, TS 103 636-{1,2,3,4,5} V2.1.1, 2024.

[3] M. Penner, M. Nabeel, and J. Peissig, "URLLC Performance Evaluation of IMT-2020 Candidate Technology: DECT-2020 New Radio," in *94th IEEE Vehicular Technology Conference (VTC2021-Fall)*, Norman, OK, USA: IEEE, Sep. 2021.

[4] "Minimum requirements related to technical performance for IMT-2020 radio interface(s)," ITU, R M.2410-0, Nov. 2017.

[5] E. Llaguno, I. Pretel, P. Angueira, and J. Montalban, "Physical Layer Performance of DECT-2020 New Radio for Factory Automation," in *2024 IEEE 20th International Conference on Factory Communication Systems (WFCS)*, Toulouse, France: IEEE, Apr. 2024.

[6] A. Samuylov et al., "Performance of MAC Layer Mechanisms in DECT-2020 NR mMTC Technology," in *99th IEEE Vehicular Technology Conference (VTC2024-Spring)*, Singapore: IEEE, Jun. 2024.

[7] R. Kovalchukov et al., "DECT-2020 New Radio: The Next Step toward 5G Massive Machine-Type Communications," *IEEE Communications Magazine*, vol. 60, no. 6, pp. 58–64, Jun. 2022.

[8] T. Nihtilä and H. Berg, "Energy Consumption of DECT-2020 NR Mesh Networks," in *2022 Joint European Conference on Networks and Communications & 6G Summit (EuCNC/6G Summit)*, Grenoble, France: IEEE, Jun. 2022, pp. 196–201.

[9] F. Graf, T. Watteyne, and M. Villnow, "What to Expect When Using DECT NR+," *IEEE Communications Magazine*, pp. 1–7, 2025.

[10] S. Mudriievskyi, F. H. P. Fitzek, and P. Seeling, "CHEAP 5G: DECT NR+ for Tactile Internet With Human In The Loop Application," in *29th European Wireless Conference (EW 2024)*, Brno, Czech Republic: VDE, Sep. 2024, pp. 31–34.

[11] M. Waßmann, A. Poets, J. Peissig, and J. Pilz, "Performance of DECT-2020 NR in an industrial environment for varying RF bands," in *2024 Joint European Conference on Networks and Communications & 6G Summit (EuCNC/6G Summit)*, Antwerp, Belgium: IEEE, Jun. 2024, pp. 610–615.

[12] Y. Dang, Q. Ngo, R. Fagerholm, V.-M. Rantanen, K. Ruttik, and R. Jäntti, "EWDC: Integrating DECT-2020 With Wi-Fi for Enhanced Wireless Direct Connectivity," *IEEE Internet of Things Journal*, vol. 12, no. 15, pp. 31 783–31 796, Aug. 2025.

[13] C. Sommer, R. German, and F. Dressler, "Bidirectionally Coupled Network and Road Traffic Simulation for Improved IVC Analysis," *IEEE Transactions on Mobile Computing*, vol. 10, no. 1, pp. 3–15, Jan. 2011.

[14] F. Bronner and C. Sommer, "Efficient Multi-Channel Simulation of Wireless Communications," in *2018 IEEE Vehicular Networking Conference (VNC)*, Taipei, Taiwan: IEEE, Dec. 2018.